Electronic structure of polyimide and related monomers: Theory and experiment

Steven P. Kowalczyk
IBM Research Division, Thomas J. Watson Research Center, P.O. Box 218, Yorktown Heights, New York 10598

Sven Stafström
Department of Physics and Measurement Technology, Linköping University, S-581 83 Linköping, Sweden

J. L. Brédas
Service de Chimie des Matériaux Nouveaux, Département des Matériaux et Procedés, Université de l'Etat à Mons, 23 avenue Maistriau, B-7000 Mons, Belgium

William R. Salaneck
Department of Physics and Measurement Technology, Linköping University, S-581 83 Linköping, Sweden

Jean L. Jordan-Sweet
IBM Research Division, Thomas J. Watson Research Center, P.O. Box 218, Yorktown Heights, New York 10598
(Received 13 September 1989)

The electronic structure of polymide and several related compounds was investigated theoretically and experimentally. The compounds include pyromellitic dianhydride, oxydianiline, and polyamic acid. Experimental electronic-structure determinations for poly(methyl phenylene oxide) and poly(vinyl methyl ketone) are also reported. The theoretical approach employed valence–effective-Hamiltonian calculations. Photoelectron spectroscopy (x-ray photoelectron spectroscopy, soft-x-ray photoelectron spectroscopy, and ultraviolet photoelectron spectroscopy) was used to experimentally measure the total valence-band density of states (VBDOS) from thin films of the above compounds. The theoretical VBDOS's were cross-section modulated to facilitate comparison with experiment. Very good agreement is found between the theoretical results and the experimental VBDOS's.

I. INTRODUCTION

Polymers in general and polyimides in particular are becoming very important in microelectronic applications.[1–4] Among the properties that are important to understand is adhesion between polyimide and other materials, especially metals. Much effort and some success has been made in trying to relate interfacial chemistry to adhesion and ultimately to intelligently control adhesion. There have been a number of fundamental surface-science studies of the interactions of metals with surfaces of polymides in the last few years.[5–9] Recently, investigations of the initial interface formation of polyimides on metal surfaces have been carried out using vapor deposition of components of polyimides[10–12] or model molecules representing parts of polyimides.[12–14] To understand the surface and interfacial chemistry, a firm knowledge of the electronic structure is necessary. Photoelectron spectroscopy has been shown to be a very good experimental tool to study polymer electronic structure.[15–17] Such understanding is also necessary simply to interpret spectra from and calculations of surfaces and interfaces.

There have already been a number of studies of polyimide, both experimental and theoretical.[18–22] Here, we extend these studies in several of ways. This work is a very closely coupled theoretical and experimental effort. The experimental approach involves high-resolution photoelectron spectroscopy, primarily x-ray photoelectron spectroscopy (XPS) and soft-x-ray photoelectron spectroscopy (SXPS) using synchrotron radiation. Also, ultraviolet-photoelectron-spectroscopy (UPS) measurements at low temperature were performed. A very beneficial feature of using these higher photon energies is that the entire valence region is observed as opposed to previous He I UPS measurement where only upper most levels are observed.[21] The theoretical approach employed is the Nicolas-Durand valence–effective-Hamiltonian (VEH) model.[22–26] An important extension here is the convolution of cross-section modulation with the theoretical density of states in the comparison with measured XPS.[27,28] The key feature is that at low photon energies (UPS) the photoionization cross section is greater for C $2p$ than for C $2s$, while at higher photon energies (XPS) the photoionization cross section is smaller for C $2p$ than for C $2s$. Another feature of this study is that we investigate not only polyimide (PI), but also the related monomers, pyromellitic dianhydride (PMDA), oxydianiline (ODA), and pthalimide (PIM). In this paper, when we refer to polyimide, we are specifically referring to PMDA-ODA polyimide (du Pont 5878). The polyimide samples included films prepared by both standard

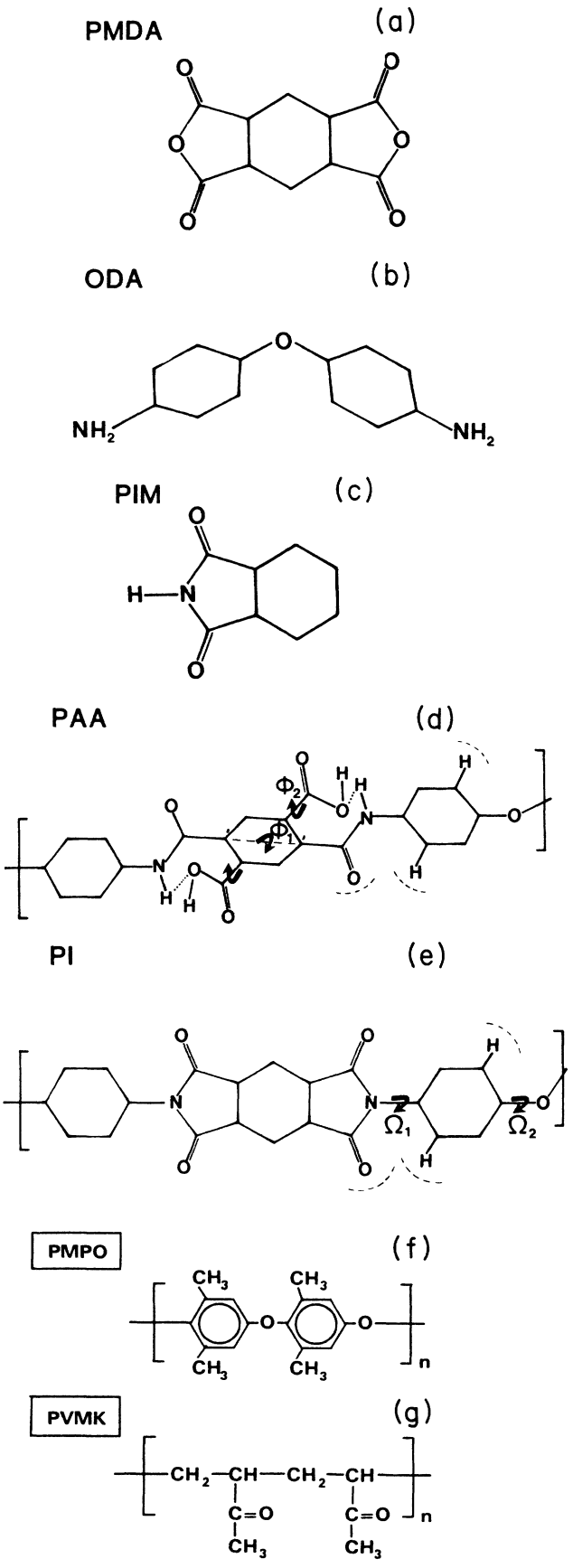

FIG. 1. Molecular structure of the compounds (a) PMDA, (b) ODA, (c) PIM, (d) PAA, (e) PI, (f) PMPO, and (g) PVMK.

solution casting techniques and a dry UHV-compatible process. We also investigated the precursor to polyimide, polyamic acid (which upon curing, i.e., thermal treatment, undergoes a condensation reaction to form polyimide). Polyamic acid is, in fact, the key chemical species involved in interfacial reactions for polyimide formed on surfaces (see Refs. 10–12). In addition, we report on experimental results for the related model polymers, poly(methyl phenylene oxide) (PMPO), which contains an ether linkage between the phenyl rings similar to the ODA part of PI, and poly(vinyl methyl ketone) (PVMK), which contains carbonyl groups as does the PMDA part of PI. Figure 1 shows the molecular repeat structures of the compounds investigated in this study.

The main purpose of this study is to understand the electronic and spectral features in photoemission spectra in the valence region of polyimide and related compounds. This information will facilitate interpretation of surface and interface studies of polyimide. Generally, we find very good agreement between our theoretical calculations and experiment.

II. EXPERIMENTAL DETAILS

Most of the samples for this study were prepared by *in situ* molecular-beam deposition (MBD). C 1*s*, N 1*s*, and O 1*s* XPS core-level spectra were used to characterize the samples. Except for PIM, room-temperature substrates were used for deposition. The PIM depositions were done at $-60\,^{\circ}\mathrm{C}$ because of its high vapor pressure at room temperature. For the vapor-deposited films, the substrates were optically flat Si wafers coated with Cu or Au. The organic films were deposited such that no substrate signal could be observed using XPS. For PMDA and ODA, quartz ovens were used. Codeposition of PMDA and ODA from individual quartz ovens was used to prepare poly(amic acid) (PAA) films.[29,30] When PAA is annealed (150–400 °C), it loses water and cycloimidizes to form a PI. The standard method of preparing PI films is to use a solution of PAA in a polar solvent followed by drying and sequential curing to 400 °C. Figure 2 shows the C 1*s* core-level–spectra characteristics of PAA and PI. We do not show other core-level spectra, since they have been discussed and analyzed elsewhere.[29–33] Our intent here is only to show one of the indications which demonstrate that the dry-processed MBD-grown films are indeed PAA and PI. Core-level spectra from PMDA and ODA films agree well with those of Grunze,[12,30] as do the PAA and PI spectra of Fig. 2.

The XPS measurements were performed on a Hewlett-Packard 5950A electron spectrometer which had been especially modified for UHV studies (base pressure $< 8.0\times10^{-10}$ Torr). Monochromatized Al $K\alpha$ x rays (1486.6 eV) were used. The photoelectron emission direction was kept fixed at 51.5° from the sample normal. The system resolution as determined from Au 4*f* core-level spectra was 0.70 eV. The system had an isolated preparation chamber where both metal and monomer depositions could be performed. Quartz ovens wrapped with a W coil were used for the depositions of the monomers and PAA, while baskets were employed for metal

depositions. One important issue that must be addressed in any XPS study of organic materials is x-ray induced damage. X-ray-induced damage was, in fact, noticed for long-term exposures (>16 h) of PMDA and ODA. The most striking evidence of radiation-induced damage came from visual inspection of the films. After the long exposures, discoloration of the films was observed. For ODA this discoloration was an image of the x-ray beam (1 mm$\times$5 mm), while for PMDA the pattern was more complex, somewhat larger than the beam size and not uniform in a pattern that suggested interference fringes. Preliminary analysis using small-area XPS analysis (150-μm spot) suggests that the ODA is fragmenting and the PMDA is evaporating under the long-term exposures.[31(b)] The PMDA and ODA spectra reported here were obtained in <2 h—before any effect of radiation-induced damage was noticeable, either visually in the films or in the spectra. No damage, either visually or in spectral line shapes, was observed for PAA or PI under any conditions employed in these investigations. Another important effect, which has to be considered in photoelectron spectroscopy of electrically insulating materials such as the ones under investigation here, is charging. There was little charging observed for films of ≈ 100 Å thickness. For films much thicker than 1000 Å, homogeneous charging was apparent. This effect produces rigid shift of all spectral features with little effect on the observed linewidth or line shape as determined by experiments using a low-energy-electron flood gun for charge compensation. In this work, we are not interested in absolute core-level binding energies, but in relative positions and intensities of characteristic features in the valence-band density of states (VBDOS). Thus, charging is not an important problem in this study. We focus mainly on the VBDOS structure, where the top of the valence band or, in fact, any well-understood feature can serve as a good fiducial for comparison with theory.

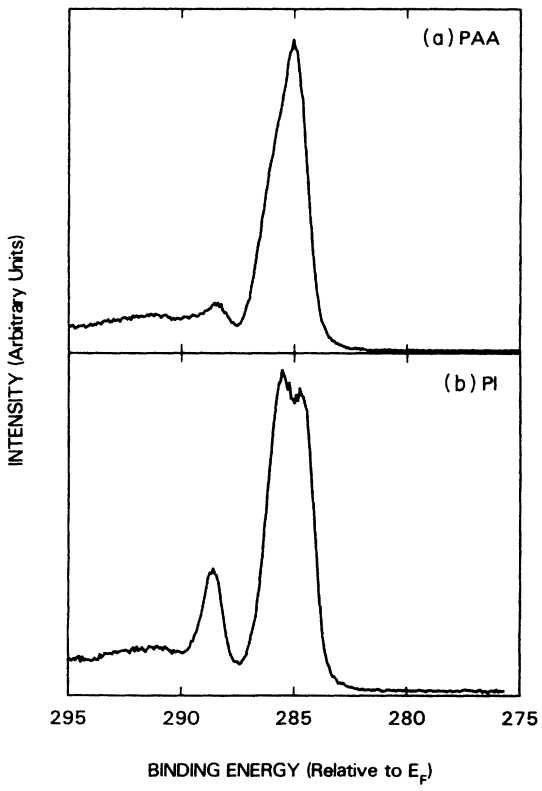

FIG. 2. C 1s core-level spectra of (a) PAA and (b) PI.

SXPS studies were done at the National Synchrotron Light Source (Brookhaven National Laboratory, Upton, NY) using a 10-m toroidal-grating monochromator in conjunction with an ellipsoidal mirror analyzer.[34] Photons in the energy range 80–500 eV were used to obtain the VBDOS spectra. MBD-grown films of PI and PAA were prepared *in situ* as discussed above for the XPS studies. Again, films were grown in a separate, isolatable UHV preparation chamber. For comparison, PI films spun-cast from solution were prepared by spinning a solution of PAA in dimethyl sulfoxide (1 g/l) onto a Cr-coated Si wafer at 6000 revolutions per minute (rpm) for 1 min and imidizing the film in vacuum at 360 °C for approximately 30 min. The PMPO films were prepared from a solution of PMPO in toluene (1.25 g/l), spun on to a Cr-coated Si(100) wafer at 2500 rpm for 1 min. These were out-gassed by heating for 40 min at about 5×10^{-10} Torr. The PVMK films were spun-cast from PVMK in methyl ethyl ketone (1 g/l) at 5000 rpm for 1 min. The spun films were in each case 50–100 Å thick.

The details of the preparation and characterization of PIM films are given in Ref. 13. The film was deposited by vapor-phase deposition onto Cu-coated, optically flat Si substrates. The UPS measurements employed an unmonochromatized He II resonance source.

III. THEORETICAL DETAILS

A. Methodology

The electronic band-structure calculations presented here were performed using the valence-effective-Hamiltonian (VEH) technique. This method was developed for molecular calculations by Nicolas and Durand[23,25] and extended for the treatment of stereoregular polymeric systems by Andre *et al.*[24] In the framework of the linear combination of atomic orbitals (LCAO) approximation, the molecular orbitals, $\psi_n(r)$, are expressed as linear combinations of atomic orbitals, $\chi_p(r-R_p)$, centered on the nuclei p:

$$\psi_n(r)=\sum_p \chi_p(r-R_p)C_{np} \ . \tag{1a}$$

In stereo-regular polymers, with cyclic boundary conditions, the crystal orbitals, $\psi_n(k,r)$ are Bloch sums of the cell (molecular) orbitals centered in cell j:

$$\psi_n(k,r)=(2N+1)^{-1/2}\sum_{j=-N}^{N}\sum_p \exp(ijka) \times\chi_p(r-R_p-ja)C_{np}(k) \ , \tag{1b}$$

where a is the length of the unit cell and $2N+1$ is the number of unit cells of the polymer chain. The LCAO-expansion coefficient matrices $\underline{C}$ and $\underline{C}(k)$ and the corresponding energy eigenvalues are obtained by solving the following sets of secular equations:

$$\underline{F}\,\underline{C}=\underline{S}\,\underline{C}E\ , \tag{2a}$$

$$\underline{F}(k)\underline{C}(k)=\underline{S}(k)\underline{C}(k)E(k)\ , \tag{2b}$$

where $\underline{F}$ and $\underline{S}$ are the Fock and overlap matrices with elements defined by

$$F_{pq}=\int \chi_q(r)h\chi_q(r-R_p)dv\ , \tag{3}$$

$$S_{pq}=\int \chi_p(r)\chi_q(r-R_q)dv\ ; \tag{4}$$

in the crystal-orbital representation the matrices $\underline{F}(k)$ and $\underline{S}(k)$ are written

$$F_{pq}(k)=\sum_{j=-N}^{N}\exp(ijka)\int \chi_p(r)h\chi_q(r-R_q-ja)dv\ , \tag{3'}$$

$$S_{pq}(k)=\sum_{j=-N}^{N}\exp(ijka)\int \chi_p(r)\chi_q(r-R_q-ja)dv\ . \tag{4'}$$

The one-electron Fock operator, h, is constructed in the VEH model as the sum of the kinetic operator and various atomic potentials, $V_A(j)$,

$$h=-\Delta/2+\sum_j\sum_A V_A(j)\ , \tag{5}$$

where the summations over j and A run over the polymer unit cells (in the molecular case this summation is excluded) and the atomic potentials present in the cell. All parameters entering a given atomic potential are optimized individually on model molecules, a procedure which permits consideration of the influence of the chemical environment.[25] The optimization process is completely theoretical and is performed in such a way as to provide polymeric or molecular energy levels of the same quality as those obtained with a Hartree-Fock *ab initio* double-ζ basis-set calculation.[25]

From the solution of Eq. (2b), the VBDOS in the polymeric case is calculated following the methodology of Delhalle and Delhalle.[36] To obtain a theoretical simulation of the XPS spectrum, it is necessary to include the relative photoionization intensities of the molecular (or crystal) orbitals into the density-of-states curve. Here use is made of the model of Gelius.[27] This model relates the photoionization intensity, I_n, of the nth molecular orbital to the Mulliken gross atomic populations and the experimental relative photoionization cross sections, σ_p, of the atomic orbitals χ_p:

$$I_n \propto \sum_p C_{np}\left[\sum_q S_{pq}C_{np}\right]\sigma_p\ . \tag{6a}$$

This relation is extended to the polymeric case as follows:[36]

$$I_n(k)\propto \sum_p C_{np}(k)\left[\sum_q S_{pq}(k)C_{nq}(k)\right]\sigma_p\ . \tag{6b}$$

The values used for σ_p are the following:[27] $\sigma(\text{O }2s)=1.4$, $\sigma(\text{O }2p)=\frac{1.4}{8}$, $\sigma(\text{N }2s)=1.2$, $\sigma(\text{N }2p)=\frac{1.2}{11}$, $\sigma(\text{C }2s)=1$, $\sigma(\text{C }2p)=\frac{1}{13}$, and $\sigma(\text{H }1s)=0$, $\sigma(\text{C }2s)$ is being taken as a reference.

The features in experimental XPS (or UPS) spectra always exhibit finite linewidths due to instrumental resolution and lifetime effects. It is therefore a common procedure to convolute the VBDOS curves by a Gaussian function whose full width at half maximum can be adjusted. The value of this broadening parameter is chosen in such a way as to obtain the best fit with the experimental linewidths. In the molecular case, each eigenstate energy is represented by such a Gaussian function, and the convoluted VBDOS curve is obtained as the sum of all of these functions.

When dealing with Hartree-Fock *ab initio* or VEH energy levels, it is necessary to perform a contraction of the total valence-band spectrum in order to obtain the best fit with experimental positions. This implies that the Hartree-Fock results usually exaggerate the total width of the valence band. The contraction factor is most easily obtained from a graphical representation of the pairs of corresponding experimental and theoretical peak positions. With such pairs represented in a Cartesian-coordinate system, the contraction factor is taken as the slope of a linear approximation to the set of points. Usually, the theoretical spectrum has to be contracted by a factor of about 1.3.[37] When comparison is made with solid-state spectra, it is also observed that a rigid shift of the theoretical VBDOS curve is needed in order to align the spectra on the energy axis. The shift is towards lower binding energy and is due to polarization of the polymer chains surrounding the chain from which an electron has been emitted (extra-atomic relaxation). This effect can not be included *a priori* in our band-structure calculations, which are performed on isolated chains. The shift is typically on the order of 2.0 eV.[37]

B. Geometry

The structure of the polyimide unit cell is shown in Fig. 1(e). All numerical values for the bond lengths and bond angles are taken from crystallographic data of equivalent geometric parameters for 4,4′-bis(phthalimide)diphenyl ether (PMDA-ODA).[38] Due to steric interactions between the close-lying oxygen and hydrogen atoms, the phenyl groups are found to be twisted by approximately 60° with respect to the phthalimide moiety in the crystal structure of this model molecule. However, a comparison between *ab initio* calculations of the C 1*s* core-level chemical shifts and experimental XPS data on polyimide model compounds has shown that the twist angle in polyimide should be somewhat smaller.[18] In order to study the effect on the electronic structure of variations in this twist angle, Ω_1 [see Fig. 1(e)], we have performed calculations using two different values, $\Omega_1=45°$ and 0°.

The ODA part of the polyimide unit cell closely resembles the unit cell of (PPO), a polymer whose crystal structure has been accurately determined.[39] In the PPO chain, all the oxygen atoms lie in the same plane and con-

secutive phenyl rings are twisted alternatively by $+45°$ and $-45°$ with respect to that plane. By analogy, we adopt the same twist angle, $\Omega_2=45°$ [see Fig. 1(e)] for the ODA part of the polyimide unit cell. We note that the choice of $\Omega_1=\Omega_2$ gives a unit cell in which the oxygen atom of the ODA moiety and the atoms of the PMDA group are all in the same plane, whereas for $\Omega_1=0°$ consecutive (all planar) PI units will be twisted alternatively by $\pm 45°$ with respect to the ether oxygen plane. In further analogy to the PPO chain, we take the C—O—C angle in the ODA part to be 124°. With this choice of polyimide geometry, the PMDA-ODA unit-cell length along the chain axis is $a=15.94$ Å (independent of the values of Ω_1 and Ω_2), in good agreement with the value of 15.4 Å reported for a fully extended PI chain.[40] It should be noted that it is necessary to perform an inversion (in this case $y \rightarrow -y$; see Fig. 1) together with the translation operation ($x \rightarrow x+a$) in order to represent the polyimide chain. Such a symmetry operation (glide-plane symmetry) can easily be performed in the VEH polymer calculation, which reduces the computational cost considerably.

The structure of PAA is sketched in Fig. 1d. The geometry we consider for this system is identical to the geometry used for PI regarding the middle phenyl ring and the ODA part. For the —CO—N—C link between these two groups, we use the bond lengths of the corresponding link in PI. The bond angles are slightly modified in order to reduce the steric interaction with the oxygen atom. For the carboxylic group (—CO—OH—), we employ the experimentally observed geometry of the corresponding group in acetic acid[41] (CH_3—CO—OH). In order to avoid the strong steric interaction between the hydrogen and oxygen atoms (which would exist for a planar conformation), we assume a twist of the middle phenyl ring around the $C' \cdots C'$ diagonal as indicated in Fig. 1(d). The twist angle we have considered here is $\phi_1=30°$. Furthermore, we assume a twist of $\phi_2=45°$ of the plane of the carboxylic group with respect to the middle phenyl ring. This twist is in a direction which increases the hydrogen-oxygen interatomic distance [indicated by a dotted line in Fig. 1(d)]. With this set of geometric parameters, the hydrogen-oxygen distance is 2.2 Å. As in the case of PI, the twist of the outer phenyl rings with respect to the same plane is $\Omega_2=45°$ and the C—O—C bond angle is 124°. The PAA unit-cell length, projected on the chain axis, is $a=17.33$ Å, somewhat longer than the experimental value of 15.9 Å reported for a chain as extended as possible. Also, for PAA, the glide-symmetry operation is performed for neighboring unit cells in order to facilitate the calculations.

For the geometries of the ODA and PMDA molecules [see Figs. 1(b) and 1(a), respectively] we take, in accordance with the geometric specifications made for PAA, the geometry corresponding to that used for the PI unit cell. Additional geometric constants necessary to specify the positions of the end oxygen atoms in PMDA, and the NH_2 groups are taken from experimental data for the corresponding group in acetic acid[41] and from standard bond length and bond angles, respectively. To test the influence of the twist angle Ω_2 on the electronic properties of ODA (as well as PI and PAA), we have performed calculations using three different values of this angle, 30°, 45°, and 60°.

IV. RESULTS

A. Experiment

In this subsection we present the experimentally obtained VBDOS's of the compounds investigated. The XPS and SXPS spectra have had their background subtracted. Figure 3 shows the XPS VBDOS from films of the monomers PMDA and ODA. Figure 4 shows the XPS VBDOS's of MBD thin films of PAA and PI. The VBDOS's of MBD PAA and PI taken at photon energies of 115, 150, 200, and 500 eV are shown in Fig. 5. The

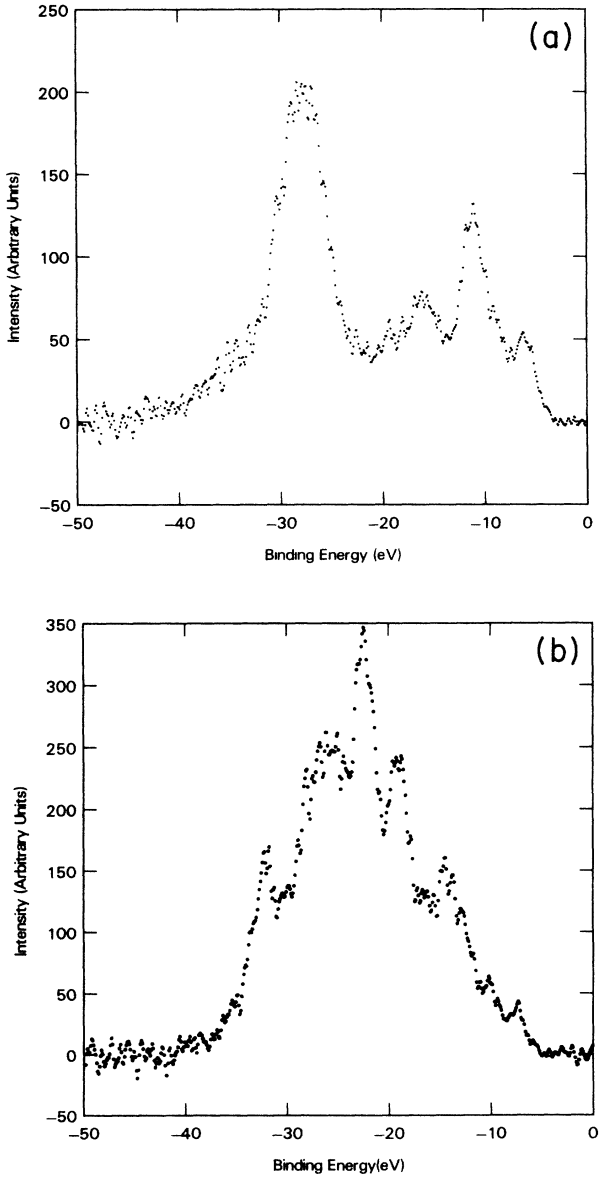

FIG. 3. XPS VBDOS's from (a) PMDA and (b) ODA.

VBDOS's taken at photon energies of 80 and 140 eV from a PI film spun-cast from solution are displayed in Fig. 6. The UPS valence-band spectrum of PIM is shown in Fig. 7. SXPS VBDOS's at photon energies of 80 and 140 eV of PPO and PMVK are shown in Fig. 8. There are a number of important observations one can make from a casual perusal of the data. The first observation is the similarity between the PI spectra from MBD films and the spun films. This confirms conclusions based on core-level spectra[29,30] that MBD films have the same electronic and chemical structure at the surface as the spun-cast films. Secondly, the cross-section variation of various features between the SXPS and XPS data is evident. These will be more fully discussed below. Also to be noted is that the PI VBDOS's are not simply a superposition

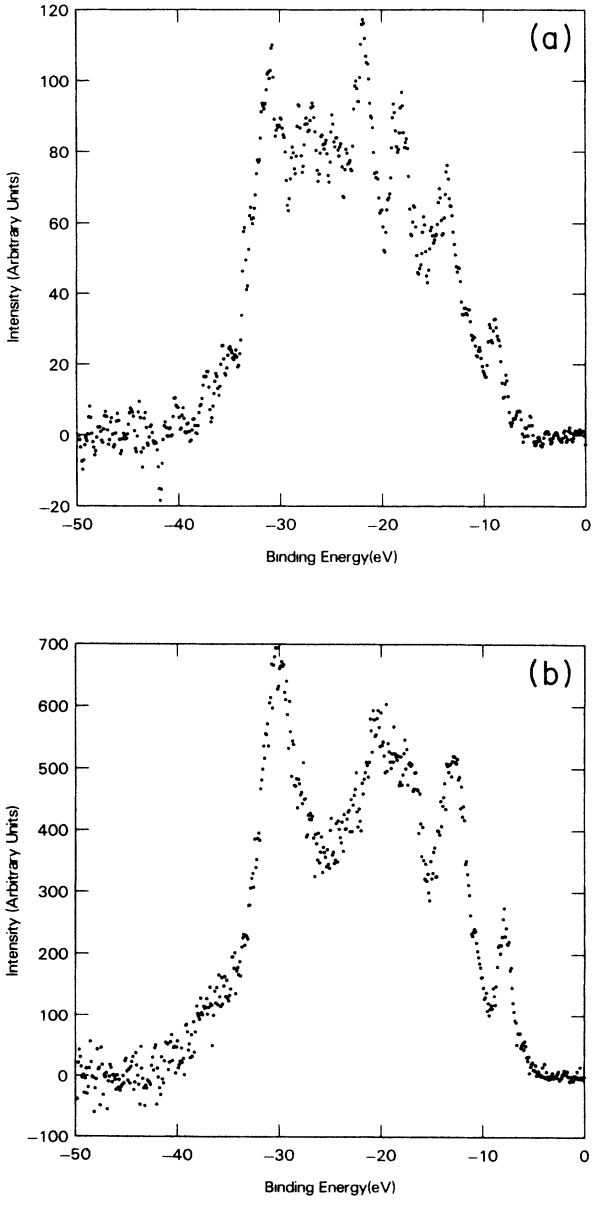

FIG. 4. XPS VBDOS's from (a) PAA and (b) PI.

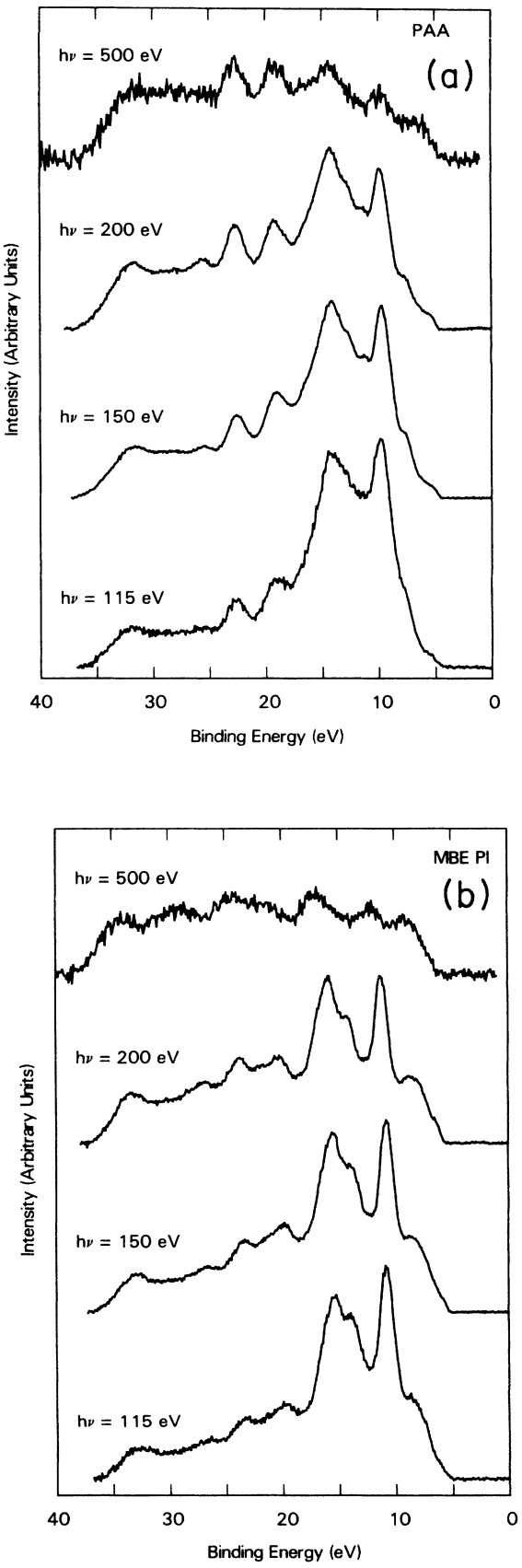

FIG. 5. SXPS VBDOS's at photon energies of 115, 150, 200, and 500 eV from films of (a) PAA and (b) PI.

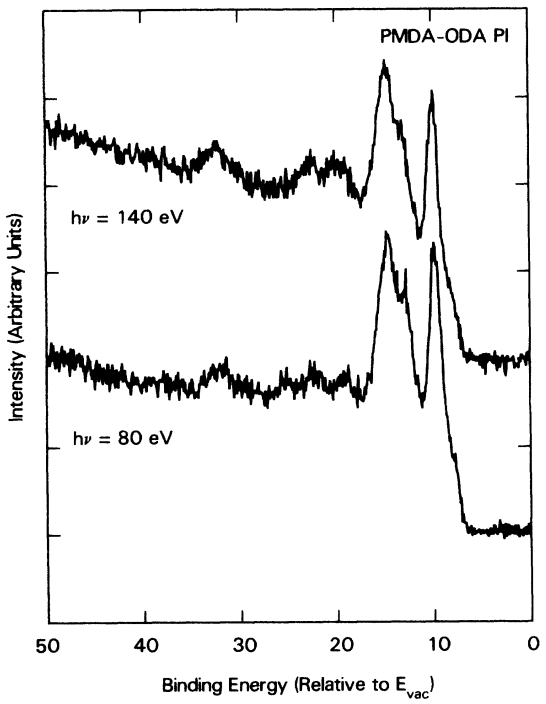

FIG. 6. SXPS VBDOS's at photon energies of 80 and 140 eV from spun-cast films of PI.

of features of the monomers PMDA and ODA. Finally, the striking similarity between the spectra of PI and the model compound PIM should be noted. A more detailed discussion will be given below, following a discussion of the theoretical calculations.

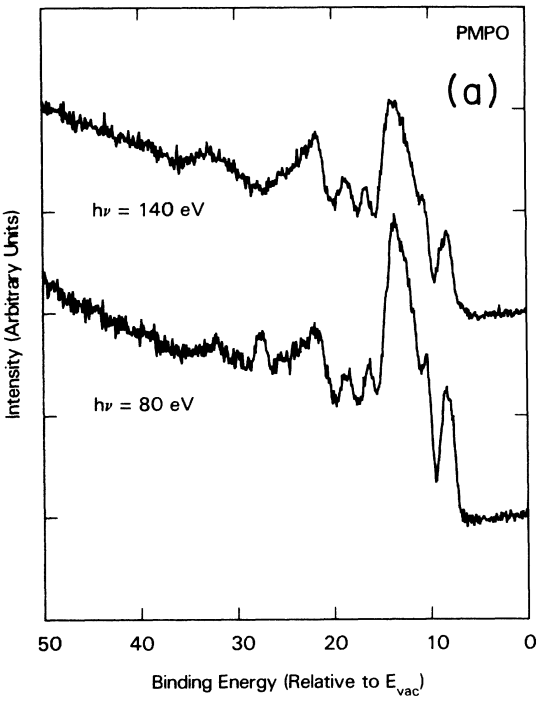

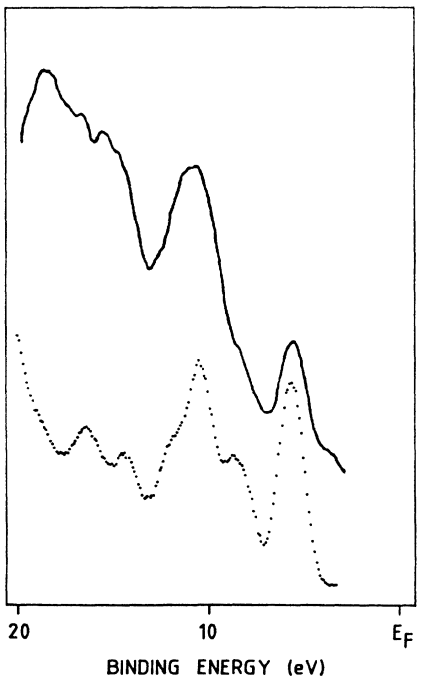

FIG. 7. UPS spectrum of the outermost valence region of PIM (·····) and, for comparison, an XPS spectrum of PI (——).

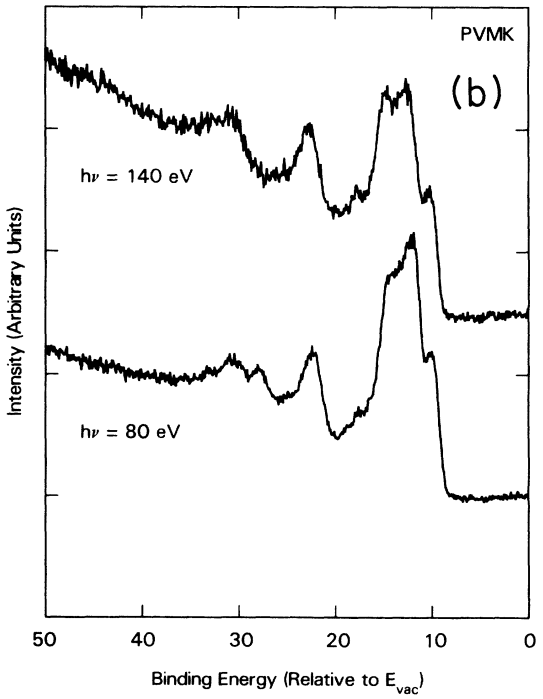

FIG. 8. (a) SXPS VBDOS's of PMPO at 80 and 140 eV photon energy. (b) SXPS VBDOS's of PVMK at 80 and 140 eV photon energy.

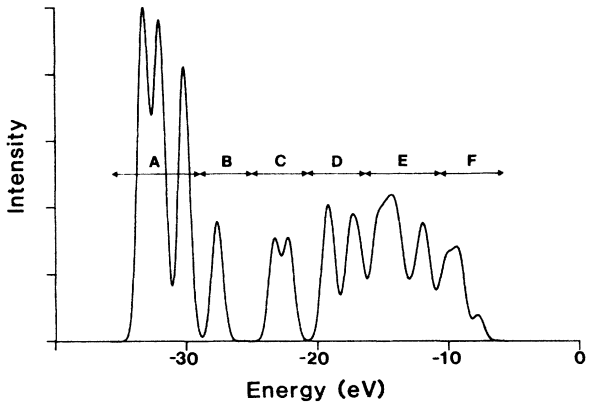

FIG. 9. VEH calculation of the VBDOS for PMDA. The VBDOS is cross-section modulated.

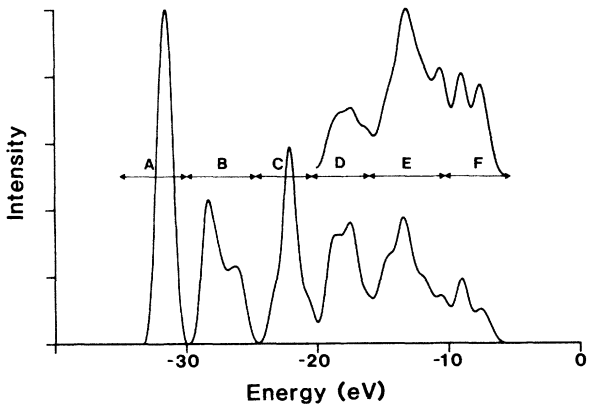

FIG. 11. VEH calculation of the VBDOS for PI. The VBDOS is cross-section modulated in the lower panel but not in the upper panel.

B. Theory

The results of the VEH calculations are shown in Figs. 9–12 for PMDA, ODA, PI, and PAA, respectively. For PMDA and ODA, we restrict the presentation to spectra including XPS cross-section effects, whereas for PI and PAA we present results both with an without such effects included. The latter are aimed at comparing with experimental SXPS results.

After having performed a linear approximation to the relation between experimental and theoretical peak positions, we find contraction coefficients within the range 1.22–1.27. For reasons of consistency, we have chosen the same contraction coefficient for all systems included in the theoretical study, namely 1.25 (i.e., the whole theoretical valence-band width is reduced by a factor of 1.25). Such a value is consistent with that used in most VEH calculations reported previously. This contraction has been performed in the spectra presented in Figs. 9–12.

In the results from the calculations performed for different Ω_1 twist angles [see Fig. 1(e)] in PI ($\Omega_1=45°$ and $\Omega_1'=0°$), there are very small changes in the VBDOS. A more careful investigation of the electronic band structure shows that the effect of decreasing the Ω_1 twist angle is to broaden the highest occupied π bands. However, the broadening is not significant since the bands are rather narrow, even for $\Omega_1'=0$. This explains the negligible effects due to changes in the twist angle on the VBDOS. Furthermore, it is also found that variation in the Ω_2 twist angle of ODA has only minor effects on the electronic properties of the molecule. Therefore, we restrict the presentation of the VBDOS to one fixed set of twist angles, namely $(\Omega_1,\Omega_2)=(45°,45°)$ in PI and $\Omega_2=45°$ in ODA. For PAA, we take $\Omega_1=45°$, $\phi_1=30°$, and $\phi_2=45°$ [see Fig. 1(d)], as described above.

V. DISCUSSION

In order to facilitate the interpretation of the theoretical valence-band density of states and the comparison with the experimental spectra, we have divided the energy axis into six regions, designated *A*–*F*. The choice of the energy intervals is such that the states in the respective regions are of similar origin. In the following, each region is discussed separately starting from the most

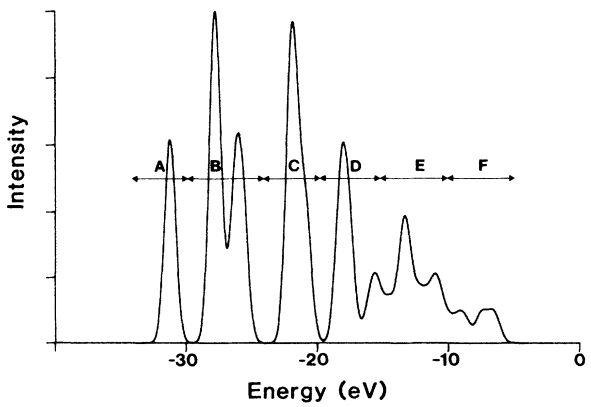

FIG. 10. VEH calculation of the VBDOS for ODA. The VBDOS is cross-section modulated.

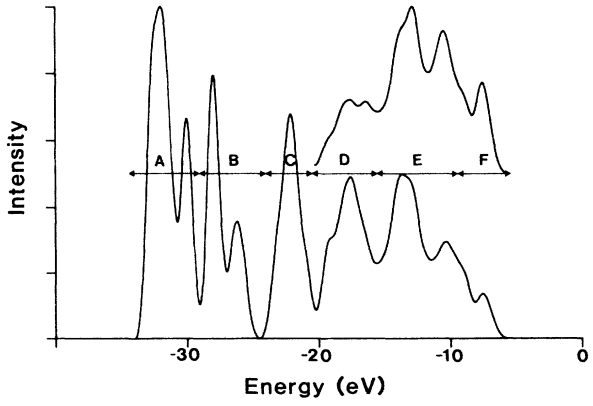

FIG. 12. VEH calculation of the VBDOS for PAA. The VBDOS is cross-section modulated in the lower panel but not in the upper panel.

tightly bound region. The cross-section-modulated theoretical spectra are designated VBDOS's. It will be explicitly stated when non-cross-section-modified spectra are discussed.

A. Region A (−35 to −30 eV)

This region of the valence-band spectrum is dominated by electrons photoemitted from molecular orbitals derived mostly from O 2*s* atomic orbitals. The number of states in the region is equal to the number of oxygen atoms for the respective systems. As clearly observed, for instance, by comparing the VBDOS's of PMDA and ODA (Figs. 9 and 10, respectively), the oxygen content of these molecules is reflected in the size and distribution of the peaks. PMDA contains six oxygen atoms whose 2*s* orbitals form eigenstates energetically grouped in pairs. This produces the three-peak structure seen in Fig. 9. The single O 2*s* orbital in ODA is observed, in comparison with PMDA, as a low-intensity peak at −31.2 eV. The comparison between the theoretical and experimental VBDOS's for PMDA and ODA is excellent. The high-binding-energy peak for PMDA is clearly much broader and more intense than the corresponding feature in ODA. Extending the comparison to the polymeric cases, we find in PI a rather narrow, but very intense, oxygen-derived peak which contains large contributions from all five of the 2*s* orbitals in the unit cell. At the low-binding-energy side of this peak we find the ether O 2*s* eigenstate at −31.2 eV, i.e., exactly the same energy as for the corresponding state in ODA. Also, the ether O 2*s* state of PAA is observed very close to this energy. Such a perfect agreement does not hold for states including O 2*s* states from the carbonyl groups, because of the different environments of these groups in PMDA, PI, and PAA. The splitting into a double-peak structure in region A for PAA, compared to the single peak for PI, is a result of such differences. This distribution of states explains the broader O 2*s* peak observed in the experimental XPS spectrum for PAA and PI.

B. Region B (−30 to −24 eV)

The main contributions to the VBDOS in this region are derived from N 2*s* orbitals. This is most clearly seen by comparing the spectral intensity in this region for PMDA and ODA (Figs. 9 and 10, respectively). The two amino nitrogen atoms in ODA give rise to the intense peak at −27.8 eV, whereas in the nitrogen-free PMDA molecule only one state (at −27.6 eV) is located in this region. This shows, however, that N 2*s* states are not the only contributors to intensity in this region. The peak in the PMDA spectrum in this region is due to a molecular orbital with a large contribution from C 2*s* and O 2*s* atomic orbitals of the C=O groups [see Fig. 3(a)]. In the ODA spectrum there are also similar states. The peak at −26.0 eV is due to states localized at the C—O and C—N groups. The theoretically obtained differences in VBDOS intensities for PMDA and ODA are clearly reflected in the experimental spectra (Fig. 3). Region B is very weak for PMDA and is dominated by the tail from Region A. For ODA, a broad and intense spectral intensity is observed throughout this region, qualitatively in agreement with the VEH VBDOS. For the polymeric cases (Figs. 11 and 12), the peaks originating from the N 2*s* atomic orbitals are found at −28.2 and −27.9 eV for PI and PAA, respectively. It should be noticed that the relative intensities between the nitrogen and oxygen peaks are quite different for the two polymers. Since the spectra are normalized by the height of the largest peak, the peaks in region B appear much weaker for PI than for PAA. This is caused by the very high intensity of the oxygen peak in PI, which contains five states in comparison with the nitrogen peak, which only contains two states. In PAA, however, each oxygen peak as well as the nitrogen peak contains two states. This explains the equal intensities of these peaks. The experimental XPS data shown in Fig. 4(a) are found to be in good agreement with these experimental observations. For PI, the region-B VBDOS merely gives rise to some structure in the tail of the oxygen peak, whereas the heights of the region-A and -B peaks are nearly identical for PAA. As in the monomer case, 2*s* contributions from C—O and C—N groups of PI and PAA are included in the peak at the low binding energy side of the B region.

C. Region C (−24 to −20 eV)

Region C is dominated by C 2*s*-derived molecular orbitals. In this region we find large differences in the VBDOS's of the two molecules, reflecting the different structure of the carbon systems. For PMDA (Fig. 9), four states grouped in pairs form two peaks at −23.3 and −20.0 eV. These states are mostly from the C 2*s* orbitals of the carbon atoms linked to each other—in this case the phenyl ring. The lower-binding-energy peak also has a contribution from $2p\sigma$-type orbitals from the outer part of the molecule. The relatively low intensity of the region-C peaks is explained by the large oxygen to carbon ratio of the PMDA molecule. Since there are six energy states associated with molecular orbitals derived from O 2*s* states in region A for the molecule, this region will be more intense than the predominantly carbon region. Note that the XPS cross section for the O 2*s* orbital is significantly larger than that for the C 2*s* orbital. For ODA, the oxygen to carbon ratio is much smaller ($\frac{1}{12}$); therefore we observe the reverse behavior, i.e., the carbon region is more intense than the oxygen region (Fig. 10). We find that the main C 2*s* peak at −21.8 eV originates from three states spread over the two phenyl rings. The low-binding-energy feature at ~21.0 eV results from more localized state on the C—N and C—O groups. Again, there is good correlation of peak positions and relative intensities between the theoretical and experimental VBDOS's. Region C is the most intense region in the XPS spectrum of ODA [Fig. 3(b)], while for PMDA [Fig. 3(a)] there is only a weak double-peak structure.

Turning to the polymer case, recall that both PAA and PI contain the phenyl parts of PMDA and ODA. Therefore, it is interesting to observe that region C for PI and PAA is well represented by a superposition of their monomer constituents, as might be expected. More ex-

plicitly, the tail at the high-binding-energy side of the main peak is dominated by the C 2*s* contribution from the middle phenyl ring, as in PMDA. In the main peak at −22.1 eV, we find contributions from the ODA part dominant, while at the low-binding-energy side $2p\sigma$ states appear which are localized at the C—O and C—N groups. Experimental and theoretical results exhibit similar intensity distributions for both PI and PAA. Again, note that the difference in region C for PAA and PI is due to the normalization of the spectra.

D. Region D (−20 to −16 eV)

In this region the $2p\sigma$ states dominate. For the ODA monomer, the peak at −18.0 eV includes four states which are best characterized as being due to extended σ states. The −19.1-eV peak has large O 2*s* and C 2*s* contributions and thus is very intense. The −17.2-eV peak arises from extended $2p\sigma$ states. The differences found theoretically for the two monomers are also well reflected in the XPS spectra. In the polymer case we find σ states that are extended either over the ODA or PMDA part. The states at the low-binding-energy side are more localized to the C—O and C—N groups. In both PAA and PI we observe σ states involving C—H groups, while in PAA there are also states from O—H and N—H groups. The contribution in the hydrogen-derives states is clearly visible from a comparison of theoretical VBDOS's with and without XPS cross-section modulation. At XPS energies the H 1*s* photoionization cross section is negligible; thus the peaks at −16.5 eV for PI and at −16.4 eV for PAA dramatically decrease compared to those features in region D calculated with the inclusion of cross-section modulation. In comparing the theoretical VBDOS's and the experimental data, we find it difficult to explain the intensity differences observed. Note that we are able to find a theoretical correspondence to the intensity between regions C and D for PI. For PAA there is clearly a dip between regions C and D experimentally as well as theoretically.

E. Region E (−16 to −10 eV)

This region has the largest density of states. Since the C 2*p* and H 1*s* character of these states is large, however, the observed XPS intensity is low. Thus a comparison with XPS and SXPS is useful in this region. For PMDA there are 16 states in this region, i.e., nearly half of the occupied states of this molecule (there are 39 doubly occupied states). Without going into details, we conclude that the ∼−12-eV peak in PMDA is due primarily to oxygen lone-pair states. The major peak at −14.3 eV contains delocalized σ states including a large portion of the C—H bonding. Two π states are also found in this region. The intensity distribution for ODA is quite different from that for PMDA. The rather sharp peak at −13.3 eV is due to two almost-degenerate states with large C 2*s* character. Except for this state, the region has low XPS intensity. There is good agreement between theoretical and experimental results in this region for the monomers.

For PI and PAA we present VBDOS's with and without cross-section modulation (Figs. 11 and 12). The latter case facilitates comparison with the SXPS results, which are more intense in this region (Figs. 5 and 6). The cross-section modulation at these energies is relatively small.

The polymers again present features similar to those of the monomers in this region. The main features appear at −13.4 and −13.6 eV for PI and PAA, respectively, and include extended σ states, oxygen lone-pair states, and a few π states. The peak at ∼−11 eV is dominated by oxygen contributions and is experimentally (both in XPS and SXPS) identified as a bump at the low-binding-energy side of the main region-D peak, clearly visible in the more oxygen-rich compounds PMDA, PAA, and PI. It is interesting to note that this feature is more intense and appears at slightly lower binding energy in PAA than in PI. This difference is observed in the experimental spectra as a smaller dip between regions E and F for PAA than for PI.

F. Region F (above −10 eV)

Since all systems presented here contain coplanar, unsaturated species, they all exhibit extended π states. Some π states have already appeared in region E, but most are in region F. In addition to the delocalized π states, there are also nitrogen and oxygen lone-pair states in region F. For PMDA, which has a large relative oxygen content, the lone pairs dominate this region and give rise to the peak at −9.4 eV. The low-binding-energy peak (−7.9 eV) is due to two extended π states. In the experimental spectrum, this peak is not clearly resolved. Instead, it is observed as the extended tail of the oxygen lone-pair peak. The ODA VBDOS is somewhat different than that for PMDA. The low-binding-energy side of region F shows a barely resolved double-peak structure in the theoretical spectrum. The states at the high-binding-energy side of this peak are π states having nodes in the para positions of the phenyl rings; therefore they do not interact with other parts of the molecule. Features at the low-binding-energy side, however, contain π states extended over the phenyl rings and the nitrogen and oxygen atoms. In the high-binding-energy side of region F there is a peak at −9.1 eV which we attribute to nitrogen lone-pair states mixed with the p_z atomic orbitals of oxygen. In the experimental spectrum of ODA we can identify all the features of the VBDOS. The barely resolved two-peak structure at the low-binding-energy side and the peak at higher binding energy are due to the nitrogen and oxygen lone-pair states.

The XPS valence-band results for the polymers are in accordance with the findings for the molecular constituents. In the XPS simulation of the VBDOS for PI, the oxygen or nitrogen lone-pair peak is found to dominate over the peak due to the π states. This is observed in the experimental XPS and SXPS spectra. However, these two peaks have almost identical intensities in the theoretical spectrum where no cross-section effects are considered. For PAA the lone-pair states are more spread out in energy, resulting in a broader peak which merges

into the low-binding-energy side of region E. This feature, as compared to PI, is qualitatively observed also in the XPS spectrum. However, by comparing the SXPS spectra for PAA and PI, the opposite trend is observed. Again, the theoretical result without cross-section effects taken into account shows a marked difference from the SXPS results.

G. Comparison of PI with model compounds

A useful approach to study polymer-metal interactions has been the use of model compounds to model various possible interactions.[7,13] PIM is a good model compound and its core-level spectra have been used to model the PI-copper interaction.[13] Figure 7 shows a direct comparison of the VBDOS of PIM with that of PI. There is quite good correlation between the two experimental VBDOS's, which further demonstrates the usefulness of PIM as a model for PI. Since we have not performed electron-structure calculations for PMPO and PVMK, we will not make any detailed discussion of their VBDOS's. There are several qualitative observations that can be made. First, in the region near the top of the valence band, approximately corresponding to region F in the above discussions, PMVK has higher relative intensity than PMPO. Secondly, in the middle region of the VBDOS, corresponding roughly to regions B–D, PMPO has greater relative intensity than PMVK. Thus, PMVK qualitatively varies relative to PMPO as PMDA varies to ODA, which is the expected behavior.

VI. CONCLUSIONS

The VBDOS's of a polyimide (PMDA-ODA), its precursor PAA, the monomers PMDA and ODA, and model compounds PIM, PMPO, and PVMK have been investigated by photoemission spectroscopy using a variety of photon energies. Electronic-structure calculations using the VEH approach including cross-section modulation were performed for PI, PAA, PMDA, and ODA. Very good agreement between theory and experiment was obtained, allowing an extensive interpretation of the VBDOS's.

The most important findings of this study can be summarized as follows. It is observed that the states at the high-binding-energy side of the valence-band spectra of PMDA, ODA, PI, and PAA are typically monatomic. The molecular orbitals in regions A, B, and C are dominated by contributions from the O $2s$, N $2s$, and C $2s$ atomic orbitals, respectively. The intensities of the peaks in the respective regions therefore serve as a measure of the oxygen, nitrogen, and carbon content of the system. For example, the PMDA molecule, which contains six oxygen atoms but no nitrogen, has a large VBDOS in region A but almost no VBDOS in region B. States including a mixture of $2s$ orbitals from different types of atoms are also formed, but are not, in general, clearly resolved in the VBDOS, since they fall into regions B and C, where the pure N $2s$ and C $2s$ states dominate. An exception is seen in the case of PMDA, for which a state with a mixture of $2s$ contributions from the carbon and oxygen atoms of the carbonyl groups appear in region B, which, in this case, does not contain any N $2s$ states.

Another characteristic property of the molecular orbitals in the high-binding-energy region of the VBDOS is that they are localized to particular subunits of the whole system. For instance, the C $2s$ orbitals of the benzene rings do not mix substantially with the C $2s$ orbitals of the carbonyl groups. This property is essential, since, by studying the changes in the VBDOS due to interactions of the system with, e.g., metals, useful information concerning the particular sites that are involved in interfacial interactions can be obtained from photoelectron spectroscopy.

As is the case for most valence-band spectra of systems containing oxygen, nitrogen, and carbon atoms, the region of intermediate binding energies, regions D and E in this case, has a high density of states originating from σ states, including mixtures of $2s$-$2p$, $2p$-$2p$, and $2p$-$1s$ (hydrogen) atomic orbitals. Therefore, individual states become less well resolved, which makes it difficult to extract detailed information concerning interfacial interactions.

Finally, the low-binding-energy region of the valence-band spectra are shown to contain π states as well as oxygen and nitrogen lone-pair states. For the systems included in this study, these different types of states group into two peaks: the one at the low-binding-energy side is dominated by the π states and that at the high-binding-energy side contains the lone-pair states. The effects on the valence band of twisting the systems, so as to reduce the overlap between the π systems on different subunits, are found to be quite weak. For the polymer systems, PI and PAA, this is because they have intrinsically quite narrow π bands, even in planar conformation. Therefore, the valence band does not yield much information concerning the values of the twist angles of these systems. However, it is highly likely that the lone-pair states, in particular, will be quite sensitive to interactions with adsorbates such as metals, since they can be stabilized by extending into the space of the metal atoms.

The detailed knowledge of the content of the individual spectral peaks presented in this investigation should be useful in interpreting valence-band spectra from polymer interfaces and should contribute to further understanding of the adhesion between polyimide and metals on a microscopic level.

ACKNOWLEDGMENTS

Part of this research was carried out at the National Synchrotron Light Source, Brookhaven National Laboratory (Upton, NY), which is supported by the U.S. Department of Energy, (Division of Materials Sciences and Division of Chemical Sciences, Office of Basic Energy Science). We are grateful to IBM Belgium, the Belgian National Fund for Scientific Research (FNRS), and

the Facultés Universitaires Notre-Dame de la Paix (FNDP) for the use of the Namur Computing Facility (SCF). One of us (S.S.) is supported by FNDP, the Swedish Natural Science Council, and the Swedish Board for Technical Development. Research in Linköping was supported in part by grants from the Swedish Natural Sciences Research Council (NER) and Imperial Chemical Industries (I.C.I.), p.l.c., United Kingdom.

[1]A. M. Wilson, in *Polyimides,* edited by K. L. Mittal (Plenum, New York, 1984), Vol. 2, p. 715.

[2]A. M. Wilson, Thin Solid Films **83**, 145 (1981).

[3]R. J. Jensen, J. P. Cummings, and H. Vora, IEEE Trans. Comp. Hybrids Manufact. Technol. **CHMT-7**, 384 (1984).

[4]C. B. Duke, Synth. Met. **21**, 5 (1987).

[5]N. J. Chou, D. W. Dong, J. Kim, and A. C. Liu, J. Electrochem. Soc. **131**, 2335 (1984).

[6]F. S. Ohuchi and S. C. Freilich, J. Vac. Sci. Technol. A **4**, 1039 (1986).

[7]J. L. Jordan, C. A. Kovac, J. F. Morar, and R. A. Pollak, Phys. Rev. B **36**, 1369 (1987).

[8]R. C. White, R. Haight, B. D. Silverman, and P. S. Ho, Appl. Phys. Lett. **51**, 481 (1987).

[9]M. J. Goldberg, J. G. Clabes, and C. A. Kovac, J. Vac. Sci. Technol. A **6**, 985 (1988); **6**, 981 (1988).

[10]S. P. Kowalczyk and J. L. Jordan-Sweet, Chem. Mater. (to be published).

[11]S. P. Kowalczyk, Y.-H. Kim, G. F. Walker, and J. Kim, Appl. Phys. Lett. **52**, 375 (1988).

[12]M. Grunze and R. N. Lamb, Chem. Phys. Lett. **133**, 283 (1987).

[13]W. R. Salaneck, S. Stafström, J. L. Brédas, S. Andersson, P. Bodö, S. P. Kowalczyk, and J. J. Ritsko, J. Vac. Sci. Technol. A **6**, 3134 (1988); S. Stafström, W. R. Salaneck, and J. L. Brédas (unpublished).

[14]M. Grunze (private communication).

[15]D. T. Clark, A. Dilks, J. Peeling, and H. R. Thomas, Faraday Soc. Discuss. **60**, 183 (1975).

[16]W. R. Salaneck, CRC Crit. Rev. Solid State Mater. Sci. **12**, 267 (1985).

[17]J. J. Pireaux, J. Riga, R. Caudano, and J. Verbist, in *Photon, Electron, and Ion Probes of Polymer Structure and Properties,* Am. Chem. Soc. Symp. Proc. No. 162, edited by D. W. Dwight, Thomas J. Fabish, and H. R. Thomas (American Chemical Society, Washington, D.C., 1981), p. 169.

[18]B. D. Silverman, P. N. Sanda, P. S. Ho, and A. R. Rossi, J. Polym. Sci. Polym. Chem. Ed. **23**, 2857 (1985).

[19]A. R. Rossi, P. N. Sanda, B. D. Silverman, and P. S. Ho, Organometallics **6**, 580 (1987).

[20]B. D. Silverman, J. W. Bartha, J. G. Clabes, P. S. Ho, and A. R. Rossi, J. Polym. Sci. Pt. A **24**, 3325 (1986).

[21]P. O. Hahn, G. W. Rubloff, and P. S. Ho, J. Vac. Sci. Technol. A **2**, 756, (1984).

[22]J. L. Brédas and T. C. Clarke, J. Chem. Phys. **85**, 253 (1987).

[23]G. Nicolas and Ph. Durand, J. Chem. Phys. **70**, 2020 (1979).

[24]J. M. Andre, L. A. Burke, J. Delhalle, G. Nicolas, and Ph. Durand, in *Proceedings of the International Symposium on Atomic, Molecular, and Solid-State Theory, Collision Phenomena, Quantum Statistics, and Computational Methods,* edited by P.-O. Löwdin and Y. Öhrn [Int. J. Quantum Chem. Symp. **13**, 283 (1979)].

[25]J. L. Brédas, R. R. Chance, R. Silbey, G. Nicolas, and Ph. Durand, J. Chem. Phys. **75**, 255 (1981).

[26]J. L. Brédas and W. R. Salaneck, J. Chem. Phys. **85**, 2219 (1986).

[27]U. Gelius, in *Electron Spectroscopy,* edited by D. A. Shirley (North-Holland, Amsterdam, 1972), p. 311.

[28]R. G. Cavell, S. P. Kowalczyk, L. Ley, R. A. Pollak, B. Mills, D. A. Shirley, and W. Perry, Phys. Rev. B **7**, 5313 (1973).

[29]J. R. Salem, F. O. Sequeda, J. Duran, W. Y. Lee, and R. M. Yang, J. Vac. Sci. Technol. A **4**, 369 (1986).

[30]M. Grunze and R. N. Lamb, J. Vac. Sci. Technol. A **5**, 1695 (1987).

[31](a) S. P. Kowalczyk (unpublished); (b) S. P. Kowalczyk (unpublished), work done using a Surface Science Instruments SSX 301 spectrometer.

[32]P. I. Buchwalter and A. I. Baise, in *Polyimides,* edited by K. L. Mittal (Plenum, New York, 1984), Vol. 1, p. 537.

[33]H. J. Leary and D. S. Campbell, Surf. Interface Anal. **1**, 75 (1979).

[34]F. J. Himpsel, Y. Jugnet, D. E. Eastman, J. J. Donelon, D. Grimm, G. Landgren, A. Marx, J. F. Morar, C. Oden, R. A. Pollak, J. Schneir, and C. Crider, Nucl. Instrum. Methods Phys. Res. **222**, 107 (1984).

[35]G. Nicolas and Ph. Durand, J. Chem. Phys. **72**, 453 (1980).

[36]J. Delhalle and S. Delhalle, Int. J. Quantum Chem. **11**, 349 (1977).

[37]J. L. Brédas, in *Handbook of Conducting Polymers,* edited by T. A. Skotheim (Dekker, New York, 1986), Vol. 2, p. 859.

[38]N. Takahashi, D. Y. Yoon, and W. Parrish, Macromolecules **17**, 2583 (1984).

[39]J. Boom and E. P. Magre, Makromol. Chem. **126**, 130 (1969).

[40]T. M. Birshtein, Vysokomol. Soedin. Ser. A **19**, 54 (1977) [Polym. Sci. U.S.S.R. **19**, 63 (1977)].

[41]J. L. Derissen, J. Mol. Struct. **7**, 67 (1971).